Supplement to:

A Diagnostic Intercomparison of Modeled Ozone Dry Deposition Over North America and Europe Using AQMEII4 Regional-Scale Simulations

Christian Hogrefe[1], Stefano Galmarini[2], Paul A. Makar[3], Ioannis Kioutsioukis[4], Olivia E. Clifton[5,6], Ummugulsum Alyuz[7], Jesse O. Bash[1], Roberto Bellasio[8], Roberto Bianconi[8], Tim Butler[9], Philip Cheung[3], Alma Hodzic[10], Richard Kranenburg[11], Aurelia Lupascu[12], Kester Momoh[7], Juan Luis Perez-Camanyo[13], Jonathan E. Pleim[1], Young-Hee Ryu[14], Roberto San Jose[13], Martijn Schaap[11], Donna B. Schwede[1,*], and Ranjeet Sokhi[7]

[1]Center for Environmental Measurement and Modeling, US Environmental Protection Agency, 109 T.W. Alexander Dr., P.O. Box 12055, RTP, NC 27711, USA
[2]JRC, European Commission, Ispra, Italy
[3]Environment and Climate Change Canada, Toronto, Canada
[4]Department of Physics, University of Patras, Patras, Greece
[5]Center for Climate Systems Research, Columbia University, New York, NY, USA
[6]NASA Goddard Institute for Space Studies, New York, NY, USA
[7]Centre for Climate Change Research (C3R), U. Hertfordshire, UK
[8]Enviroware srl, Concorezzo, MB, Italy
[9]Research Institute for Sustainability – Helmholtz Centre Potsdam, Germany
[10]NCAR, Boulder, CO, USA
[11]TNO, Utrecht, the Netherlands
[12]ECMWF, Bonn, Germany
[13]Technical University of Madrid (UPM), Madrid, Spain
[14]Yonsei University, Seoul, South Korea
[*]retired

Correspondence to: Christian Hogrefe (hogrefe.christian@epa.gov)

Table of Contents

Table S1: WRF/CMAQ STAGE mapping of the dry deposition module LU categories (AQMEII4) from the LSM LU categories (MODIS for the U.S. EPA simulations over North America, MODIS + extended urban categories over the greater London area for the University of Hertfordshire simulations over Europe)

Dry Deposition LU	LSM LU
1: Water	17: water
2: Developed / Urban	13: Urban and Built-up Additional urban categories over the greater London area for the University of Hertfordshire WRF/CMAQ STAGE simulations
3: Barren	16: Barren or Sparsely Vegetated
4: Evergreen needleleaf forest	1: Evergreen Needleleaf Forest
5: Deciduous needleleaf forest	3: Deciduous Needleleaf Forest
6: Evergreen broadleaf forest	2: Evergreen Broadleaf Forest
7: Deciduous broadleaf forest	4: Deciduous Broadleaf Forest
8: Mixed forest	5: Mixed Forest
9: Shrubland	6: Closed Shrublands; 7: Open Shrublands
10: Herbaceous	N/A
11: Planted / Cultivated	12: Croplands 14: Cropland-Natural Vegetation Mosaic
12: Grassland	10: Grasslands
13: Savanna	8: Woody Savanna 9: Savanna
14: Wetlands	11: Permanent Wetlands
15: Tundra	18: Wooded Tundra 19: Mixed Tundra 20: Barren Tundra
16: Snow and Ice	15: Snow and Ice

Table S2. GEM-MACH (Base) and GEM-MACH (Ops) mapping of the dry deposition module LU categories (Robichaud/Wesely 1989) from the LSM LU categories (Zhang 2003)

Dry Deposition LU	LSM LU
1: Evergreen needleleaf forest	4: Evergreen needleleaf trees
2: Evergreen broadleaf forest	5: Evergreen broadleaf trees 8: Tropical broadleaf trees
3: Deciduous needleleaf forest	6: Deciduous needleleaf trees
4: Deciduous broadleaf forest	7: Deciduous broadleaf trees 9: Drought deciduous trees
5: Mixed Forest	25: Mixed Wood Forest
6: Grassland	14: Long grass
7: Crops, mixed farming	15:Crops 17: Sugar 18: Maize 19: Cotton 20: Irrigated Crops
8: Desert	24: Desert
9: Tundra	22: Tundra
10: Dwarf trees, shrubs	10: Evergreen broadleaf shrubs 11: Deciduous shrubs 12: Thorn shrubs 13: Short grass and forbs 26: Mixed Shrubs
11: Wetland with plants	22: Swamp
12: Ice caps and glaciers	2: Ice
13: Inland water	3: Inland Lake (Fresh)
14: Ocean	1: Water (Ocean)
15: Urban	21: Urban

Table S3. WRF/Chem (RIFS) mapping of the dry deposition module LU categories (USGS24) from the LSM LU categories (CORINE)

Dry Deposition LU	LSM LU
1: Urban and Built-Up Land	31: Low Intensity Residential 32: High Intensity Residential 33: Industrial or Commercial
2: Dryland Cropland and Pasture	2: Dryland Cropland and Pasture
3: Irrigated Cropland and Pasture	3: Irrigated Cropland and Pasture;
4: Mixed Dryland/Irrigated Cropland and Pasture	4: Mixed Dryland/Irrigated Cropland and Pasture
5: Cropland / Grassland Mosaic	5: Cropland/Grassland Mosaic;
6: Cropland / Woodland Mosaic	6: Cropland/Woodland Mosaic
7: Grassland	7: Grassland
8: Shrubland	8: Shrubland
9: Mixed Shrubland / Grassland	9: Mixed Shrubland / Grassland
10: Savanna	10: Savanna
11: Deciduous Broadleaf Forest	11: Deciduous Broadleaf Forest
12: Deciduous Needleleaf Forest	12: Deciduous Needleleaf Forest
13: Evergreen Broadleaf Forest	13: Evergreen Broadleaf Forest
14: Evergreen Needleleaf Forest	14: Evergreen Needleleaf Forest
15: Mixed Forest	15: Mixed Forest
16: Water Bodies	16: Water Bodies
17: Herbaceous Wetland	17: Herbaceous Wetland
18: Wooded Wetland	18: Wooded Wetland
19: Barren or Sparsely Vegetated	19: Barren or Sparsely Vegetated
20: Herbaceous Tundra	20: Herbaceous Tundra
21: Wooded Tundra	21: Wooded Tundra
22: Mixed Tundra	22: Mixed Tundra
23: Bare Ground Tundra	23: Bare Ground Tundra
24 Snow or Ice	24: Snow or Ice

Table S4: WRF/Chem (NCAR) mapping of the dry deposition module LU categories (USGS24) from the LSM LU categories (MODIS)

Dry Deposition LU	LSM LU
1: Urban and Built-Up Land	13 Urban and Built-Up
2: Dryland Cropland and Pasture	N/A
3: Irrigated Cropland and Pasture	N/A
4: Mixed Dryland/Irrigated Cropland and Pasture	12 Croplands
5: Cropland / Grassland Mosaic	14 cropland/natural vegetation mosaic
6: Cropland / Woodland Mosaic	N/A
7: Grassland	10: Grasslands
8: Shrubland	6: Closed Shrublands
9: Mixed Shrubland / Grassland	7: Open Shrublands
10: Savanna	8: Woody Savannas 9: Savannas
11: Deciduous Broadleaf Forest	4: Deciduous Broadleaf Forest
12: Deciduous Needleleaf Forest	3: Deciduous Needleleaf Forest
13: Evergreen Broadleaf Forest	2: Evergreen Broadleaf Forest
14: Evergreen Needleleaf Forest	1: Evergreen Needleleaf Forest
15: Mixed Forest	5: Mixed Forests
16: Water Bodies	17: Water
17: Herbaceous Wetland	11: Permanent wetlands
18: Wooded Wetland	N/A
19: Barren or Sparsely Vegetated	16: Barren or Sparsely Vegetated 20: Barren Tundra
20: Herbaceous Tundra	N/A
21: Wooded Tundra	18: Wooded Tundra
22: Mixed Tundra	19: Mixed Tundra
23: Bare Ground Tundra	N/A
24: Snow or Ice	15: Snow and Ice

Table S5: WRF/CMAQ (STAGE) (EU4) mapping of the dry deposition module LU categories (AQMEII4) from the LSM LU categories (MODIS + U.K. Urban)

Dry Deposition LU	LSM LU
1: Water	17: water
2: Developed / Urban	13: Urban and Built-up 31: Low Intensity Residential (present only for London) 32: High Intensity Residential (present only for London) 33: Industrial or Commercial (not present in domain)
3: Barren	16: Barren or Sparsely Vegetated
4: Evergreen needleleaf forest	1: Evergreen Needleleaf Forest
5: Deciduous needleleaf forest	3: Deciduous Needleleaf Forest
6: Evergreen broadleaf forest	2: Evergreen Broadleaf Forest
7: Deciduous broadleaf forest	4: Deciduous Broadleaf Forest
8: Mixed forest	5: Mixed Forest
9: Shrubland	6: Closed Shrublands 7: Open Shrublands
10: Herbaceous	N/A
11: Planted / Cultivated	12: Croplands 14: Cropland-Natural Vegetation Mosaic
12: Grassland	10: Grasslands
13: Savanna	8: Woody Savanna 9: Savanna
14: Wetlands	11: Permanent Wetlands
15: Tundra	18: Wooded Tundra 19: Mixed Tundra 20: Barren Tundra
16: Snow and Ice	15: Snow and Ice

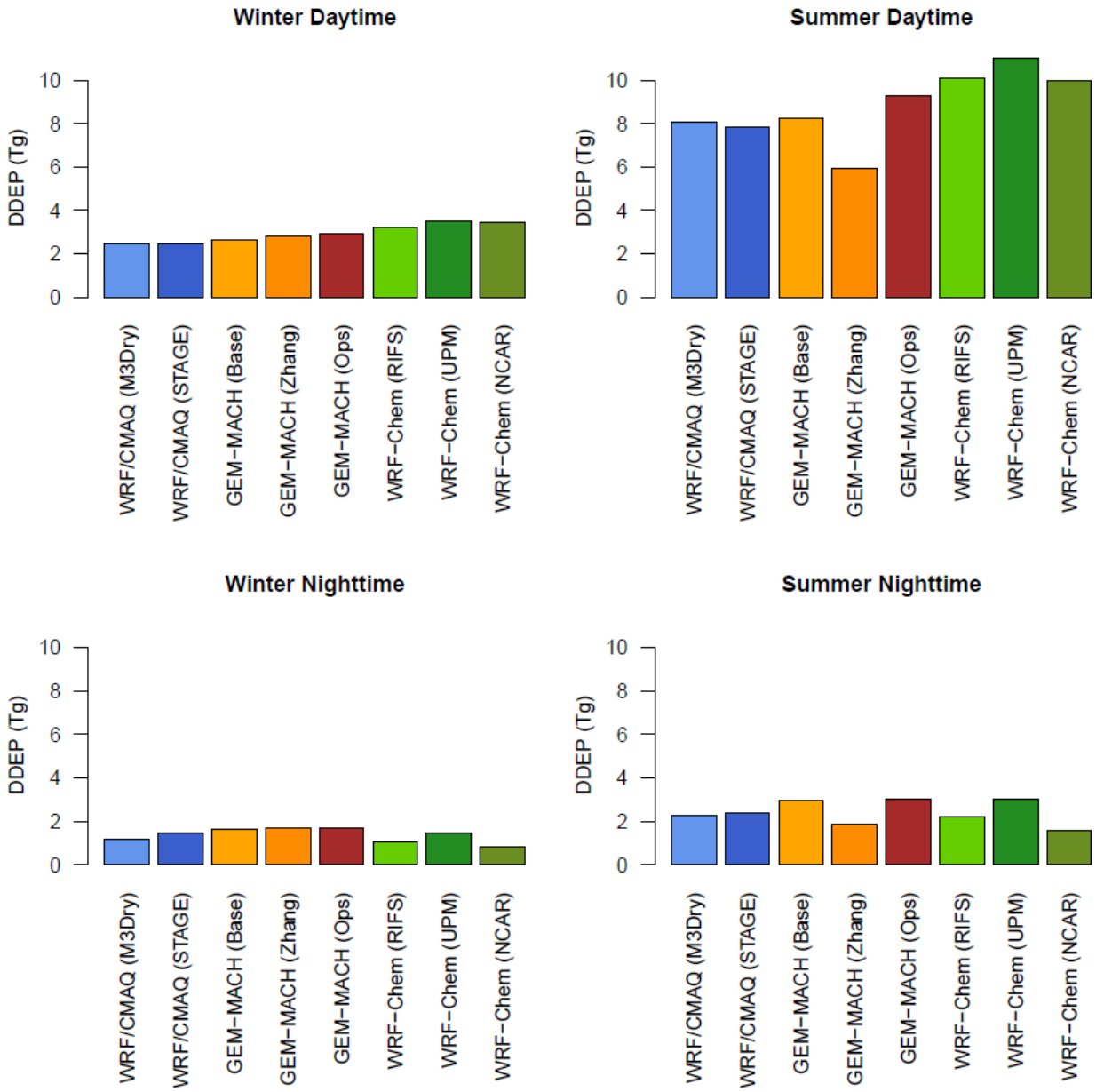

Figure S1: Seasonal and diurnal variations in 2016 NA domain total O_3 grid-scale dry deposition fluxes (in Tg). Totals are calculated over all non-water grid cells in the analysis domain common to all models. Daytime values are calculated from 10:00 LST to 14:00 LST while nighttime values are calculated from 22:00 LST to 02:00 LST. a) winter daytime, b) summer daytime, c) winter nighttime, d) summer nighttime

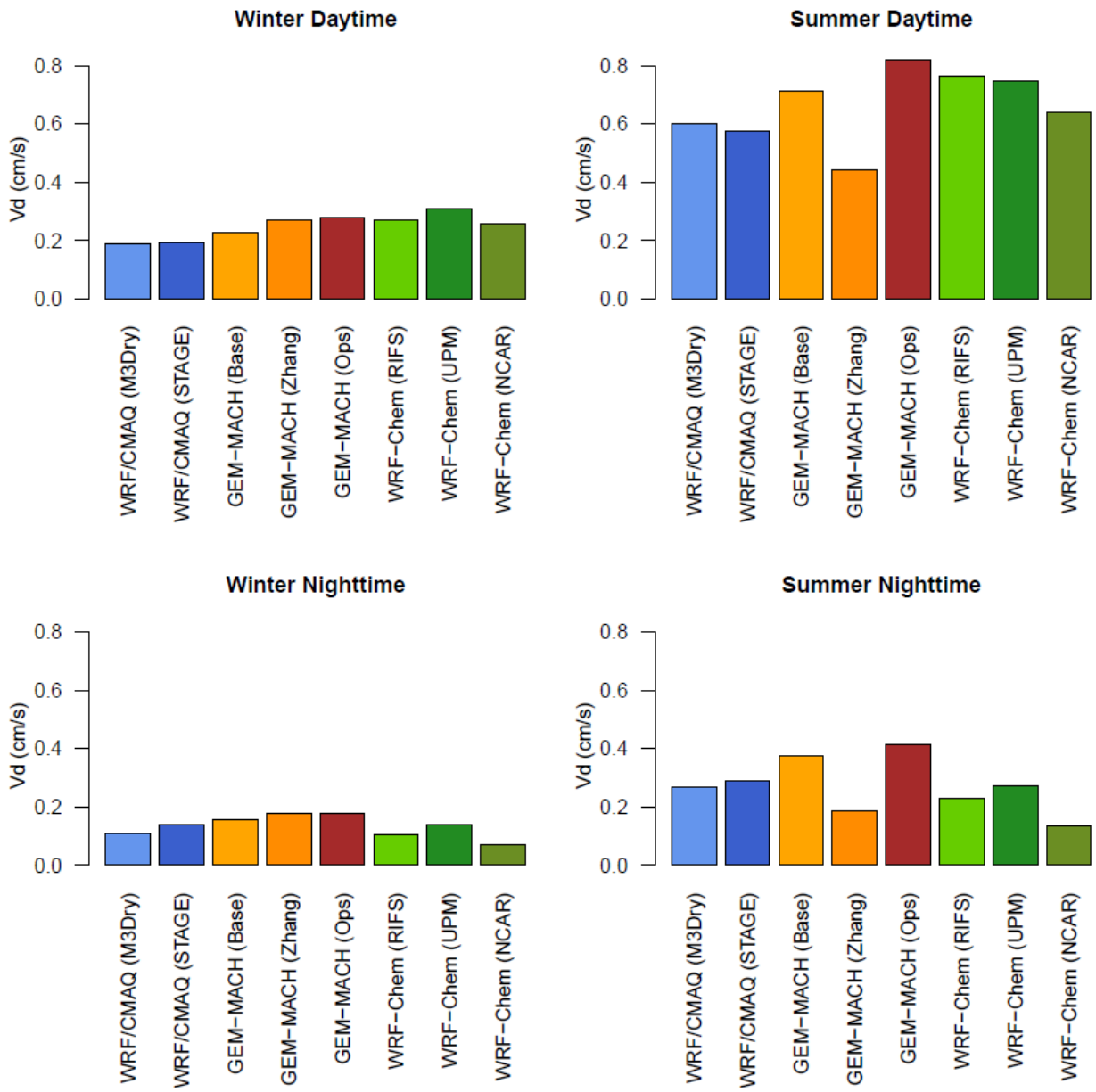

Figure S2: Seasonal and diurnal variations in 2016 NA domain average O_3 grid-scale dry deposition velocities (in cm/s). Averages are calculated over all non-water grid cells in the analysis domain common to all models. Daytime values are calculated from 10:00 LST to 14:00 LST while nighttime values are calculated from 22:00 LST to 02:00 LST. a) winter daytime, b) summer daytime, c) winter nighttime, d) summer nighttime

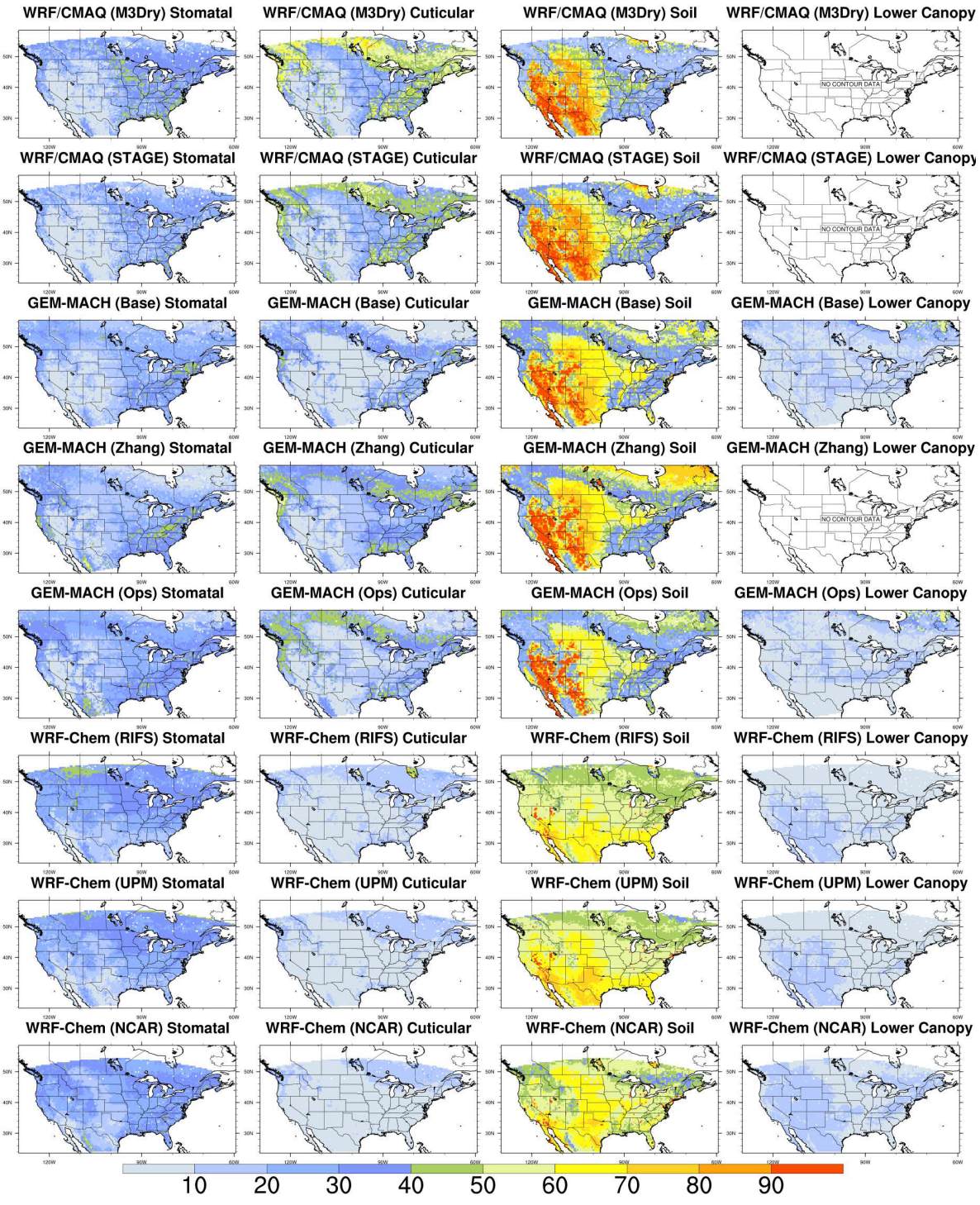

Figure S3: Percentage contributions of grid-scale ozone effective conductances to the sum of all pathways, averaged over the entire year. Results are for the NA domain during 2016. Note that these maps are not clipped to the domain common to all simulations and show the maximum spatial extent of non-water cells submitted for each model.

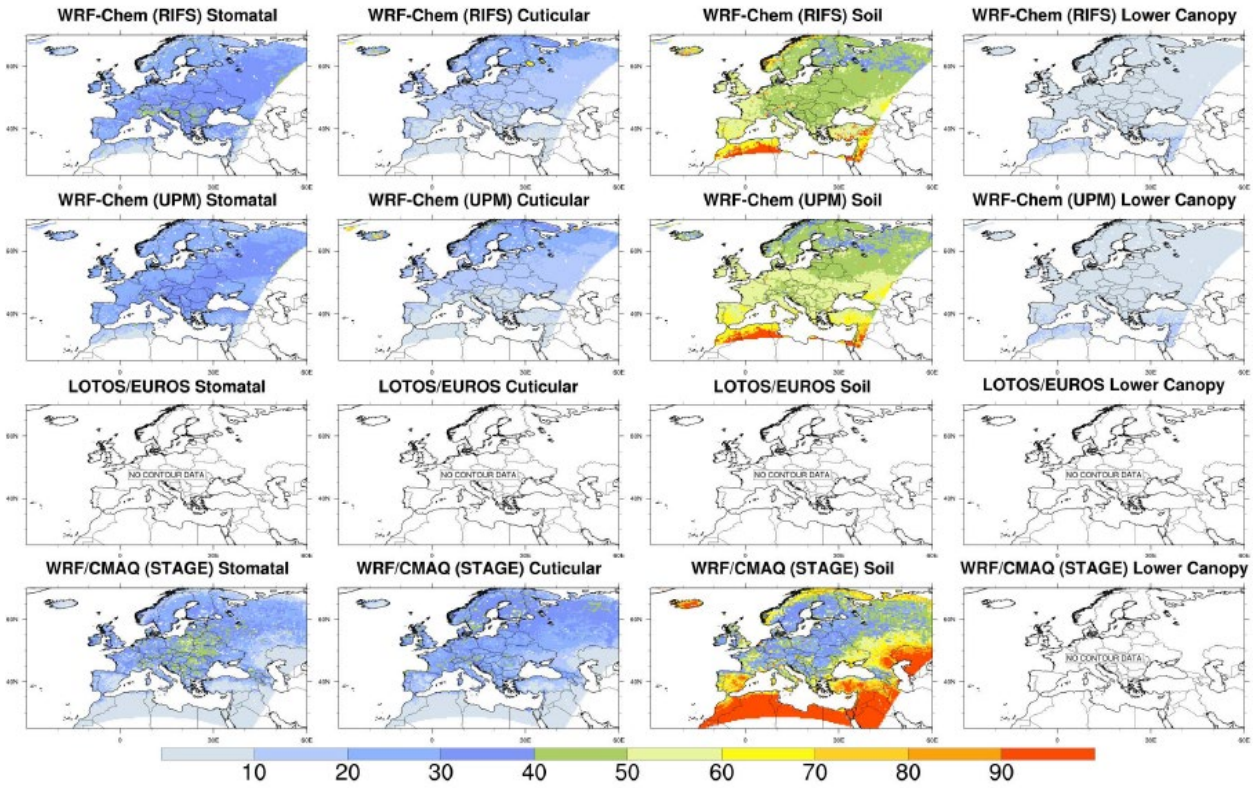

155

Figure S4: Percentage contributions of grid-scale ozone effective conductances to the sum of all pathways, averaged over the entire year. Results are for the EU domain during 2010. Note that these maps are not clipped to the domain common to all simulations and show the maximum spatial extent of non-water cells submitted for each model.

160

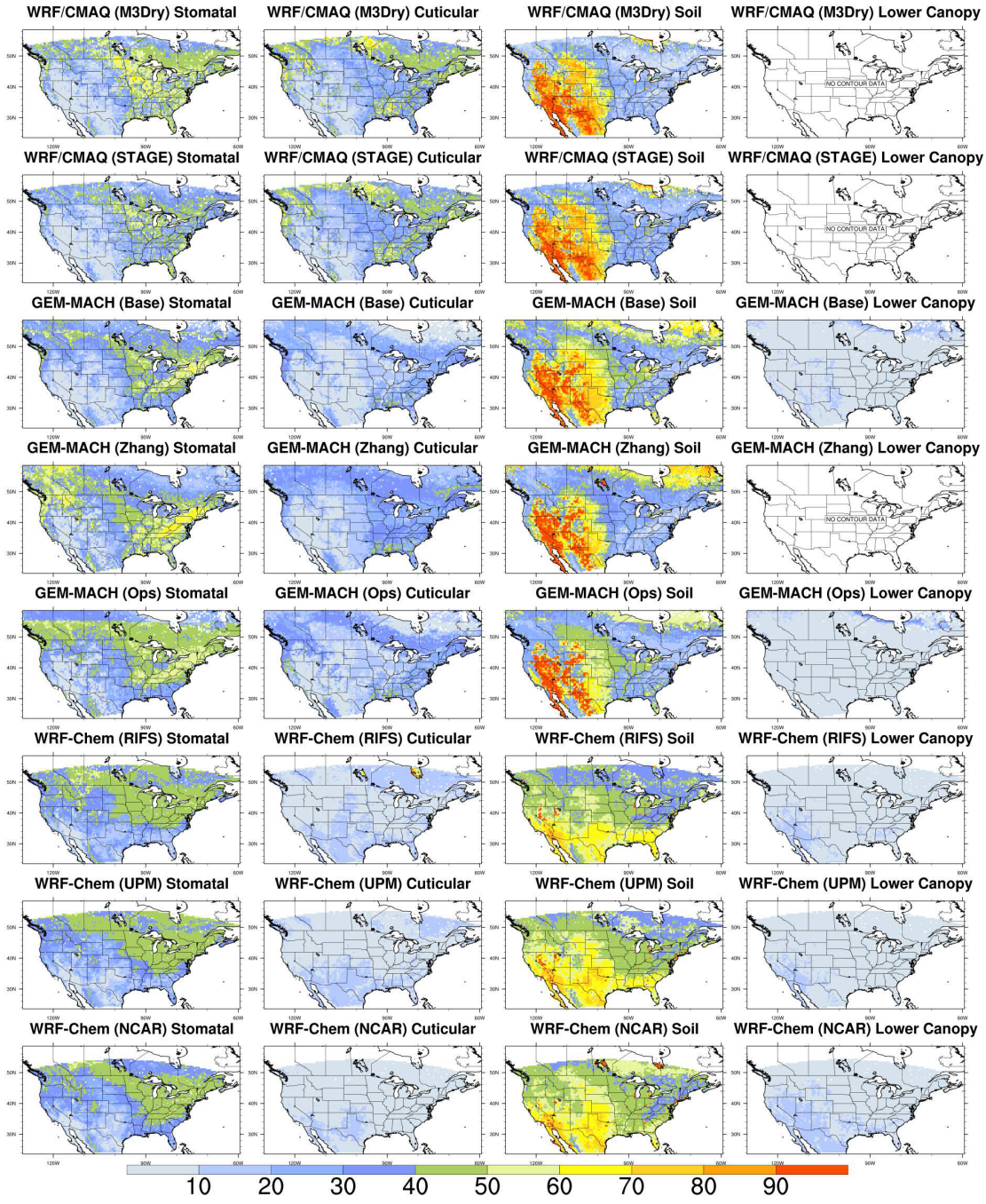

Figure S5. Percentage contributions of grid-scale ozone effective conductances to the sum of all pathways, averaged over all hours during summer. Results are for the NA domain during 2016. Note that these maps are not clipped to the domain common to all simulations and show the maximum spatial extent of non-water cells submitted for each model.

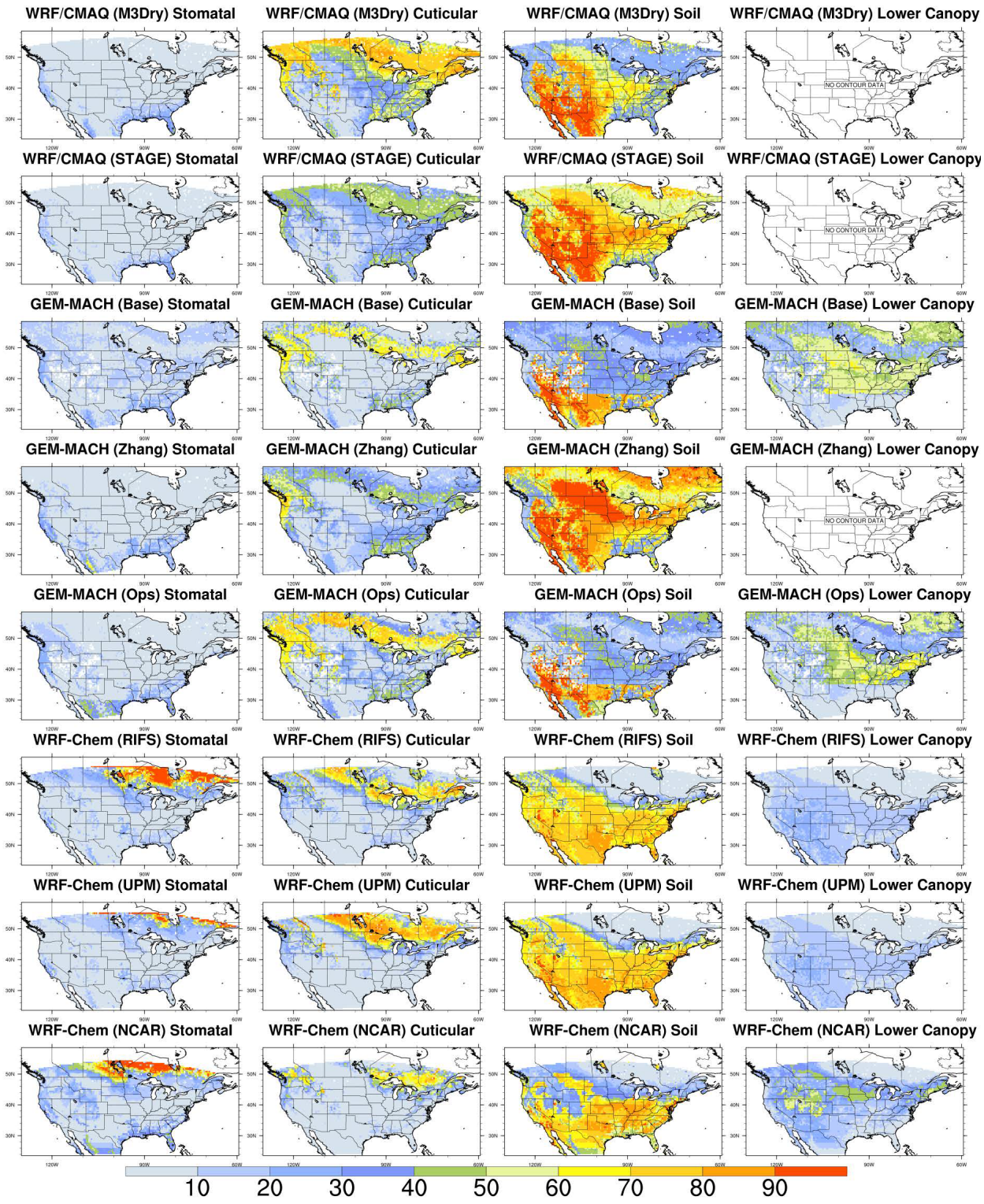

Figure S6: As in Figure S5 but for winter.

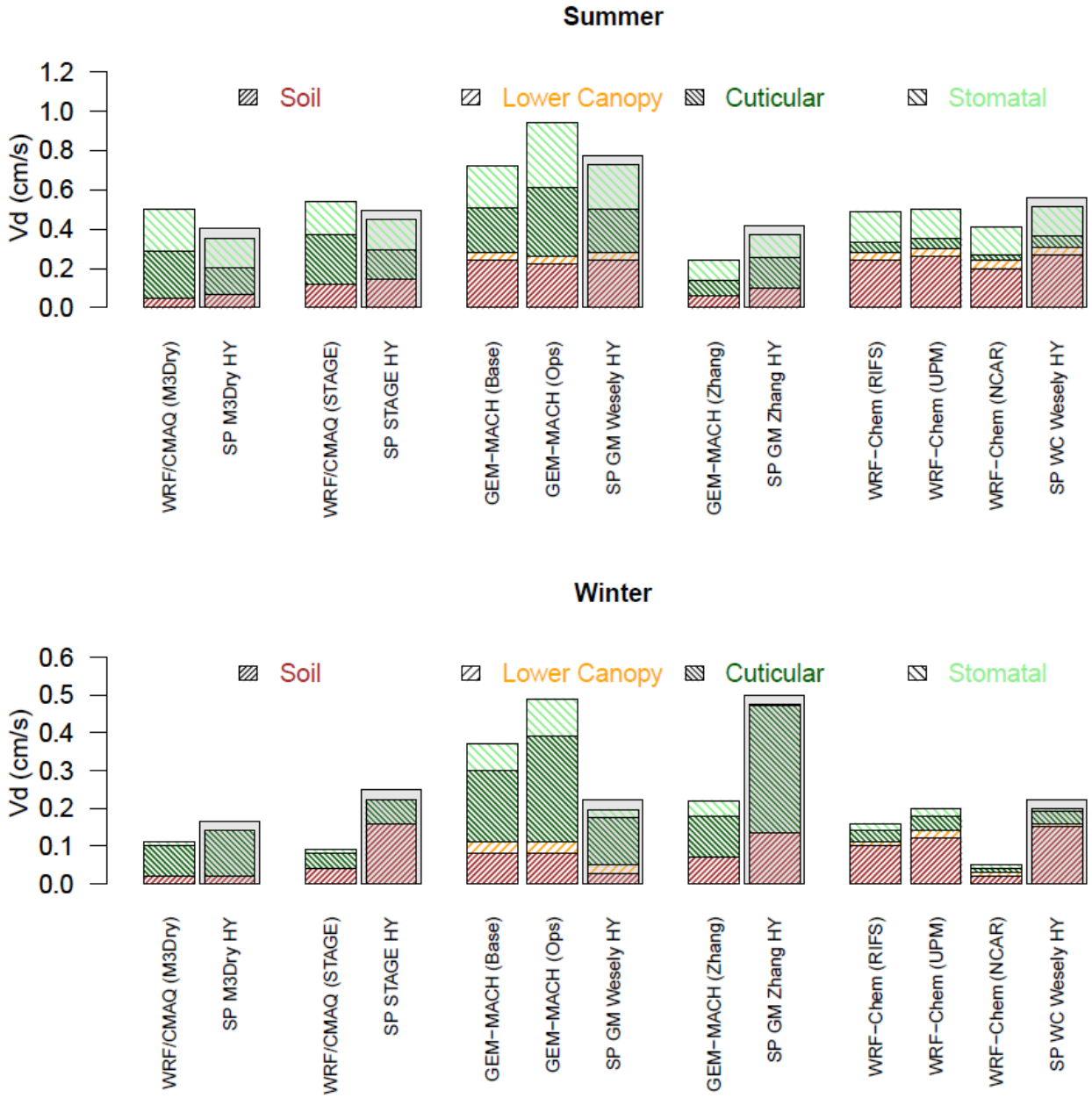

Figure S7: Summer and winter effective conductances and ozone deposition velocities calculated by the grid models for evergreen needleleaf forest grid cells and calculated by the corresponding subset of single point (SP) models analyzed in Clifton et al. (2023) at the Hyytiälä (HY) site. In the x-axis labels, results for the SP GEM-MACH Wesely simulations are shown as "SP GM Wesely" while results for the SP WRF-Chem Wesely simulations are shown as "SP WC Wesely". The evergreen needleleaf forest grid cells selected for this analysis are those in which a given model had at least 85% coverage for this LU category. The number of these grid cells differs across models due to underlying differences in LU (see Section 3.3).

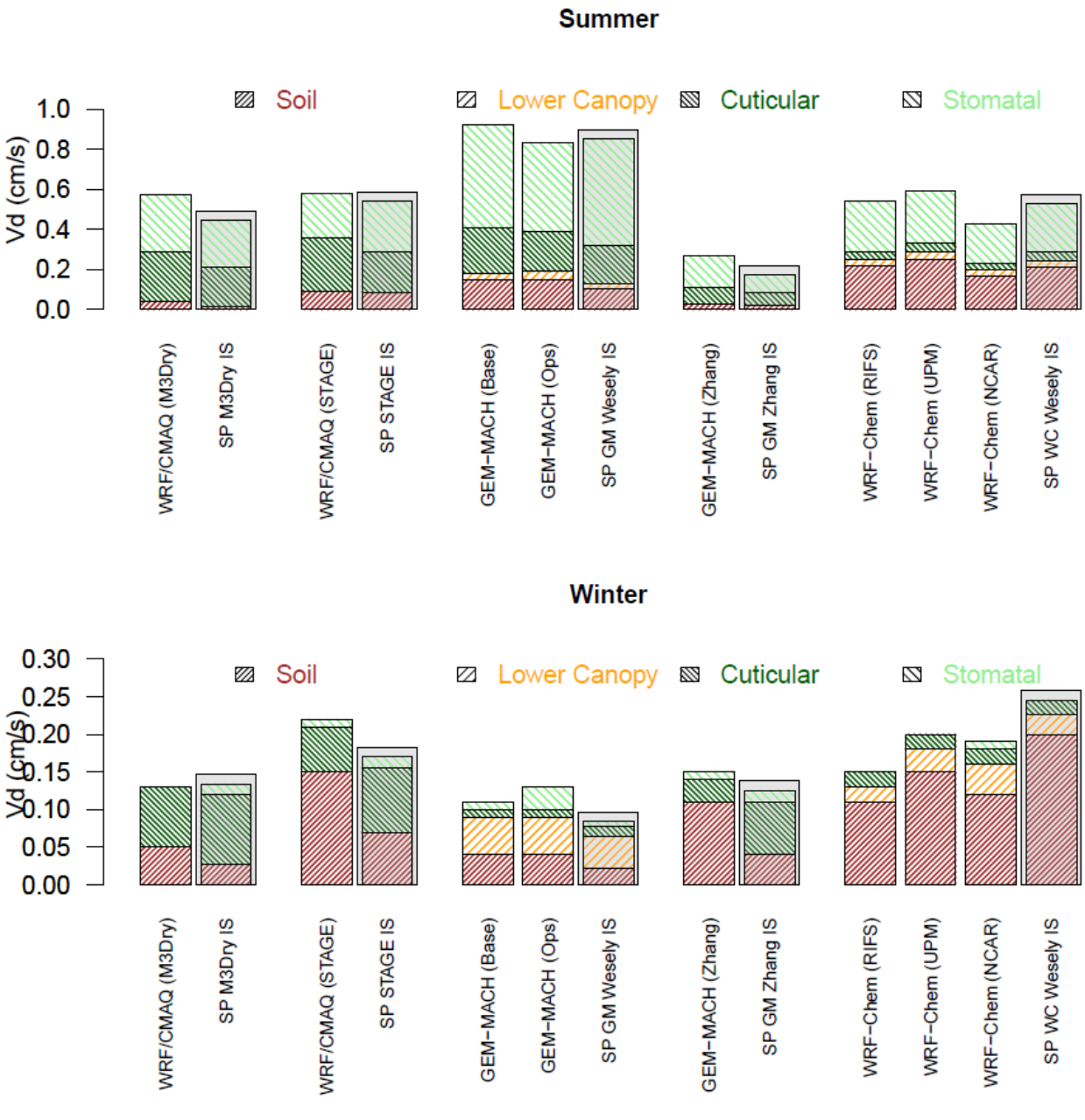

Figure S8: Summer and winter effective conductances and ozone deposition velocities calculated by the grid models for deciduous broadleaf forest grid cells and calculated by the corresponding subset of single point (SP) models analyzed in Clifton et al. (2023) at the Ispra (IS) site. In the x-axis labels, results for the SP GEM-MACH Wesely simulations are shown as "SP GM Wesely" while results for the SP WRF-Chem Wesely simulations are shown as "SP WC Wesely". The deciduous broadleaf forest grid cells selected for this analysis are those in which a given model had at least 85% coverage for this LU category. The number of these grid cells differs across models due to underlying differences in LU (see Section 3.3).

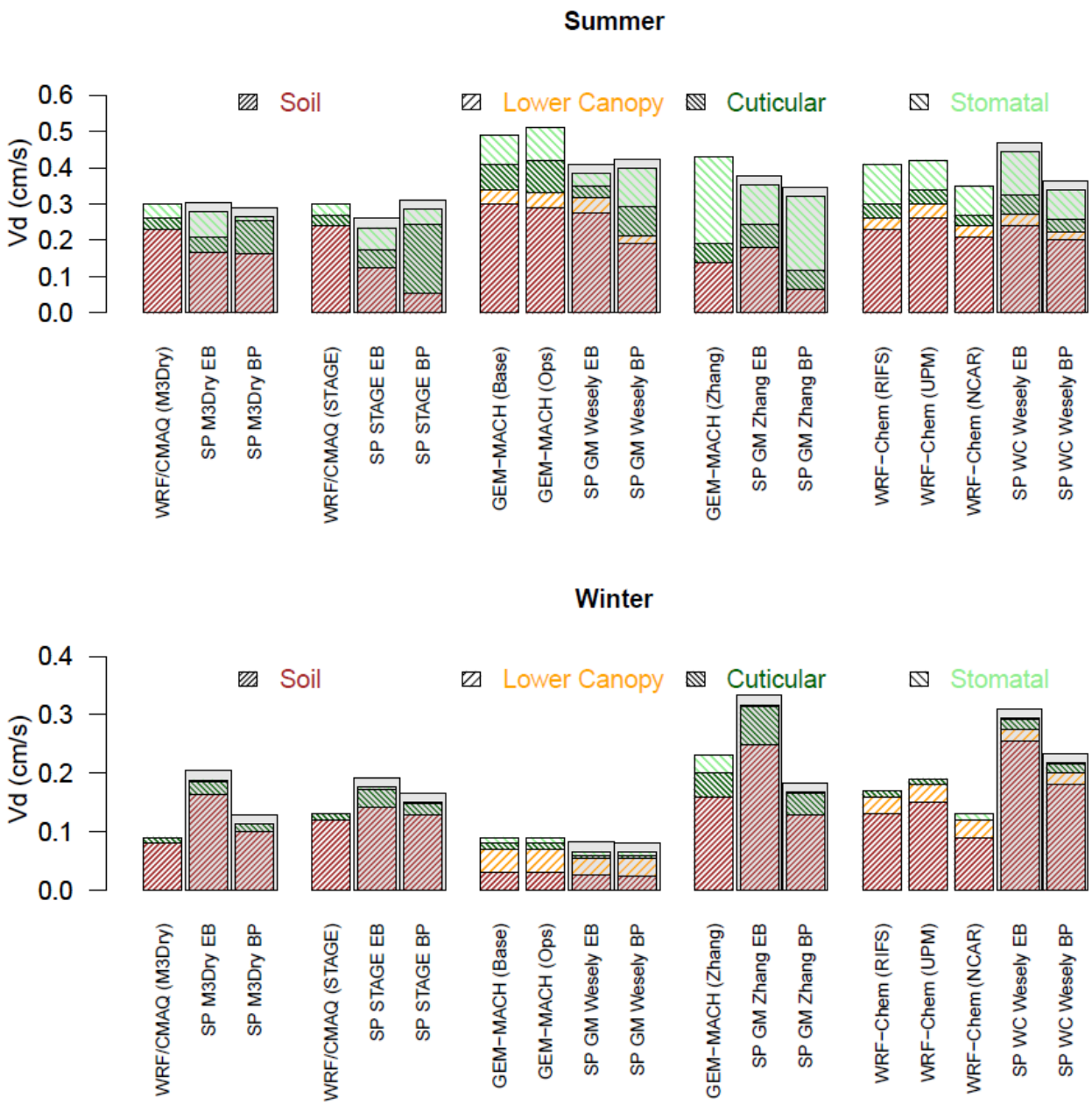

Figure S9: Summer and winter effective conductances and ozone deposition velocities calculated by the grid models for grassland grid cells and calculated by the corresponding subset of single point (SP) models analyzed in Clifton et al. (2023) at the Easter Bush (EB) and Bugacpuszta (BP) sites. In the x-axis labels, results for the SP GEM-MACH Wesely simulations are shown as "SP GM Wesely" while results for the SP WRF-Chem Wesely simulations are shown as "SP WC Wesely". The grassland grid cells selected for this analysis are those in which a given model had at least 85% coverage for this LU category. The number of these grid cells differs across models due to underlying differences in LU (see Section 3.3).

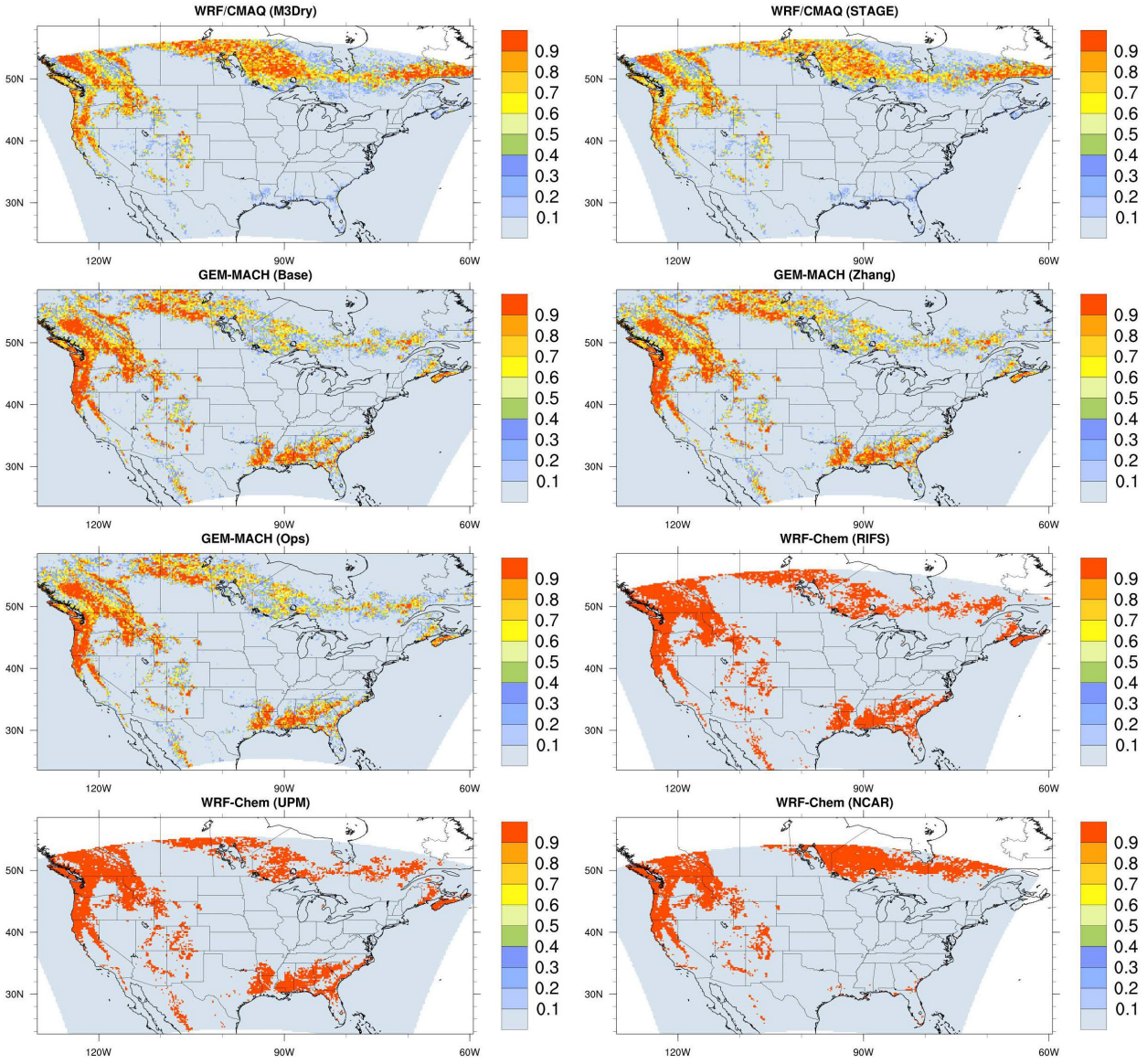

200 **Figure S10: Fractional coverage of the evergreen needleleaf forest LU category for each of the participating models over the NA domain.**

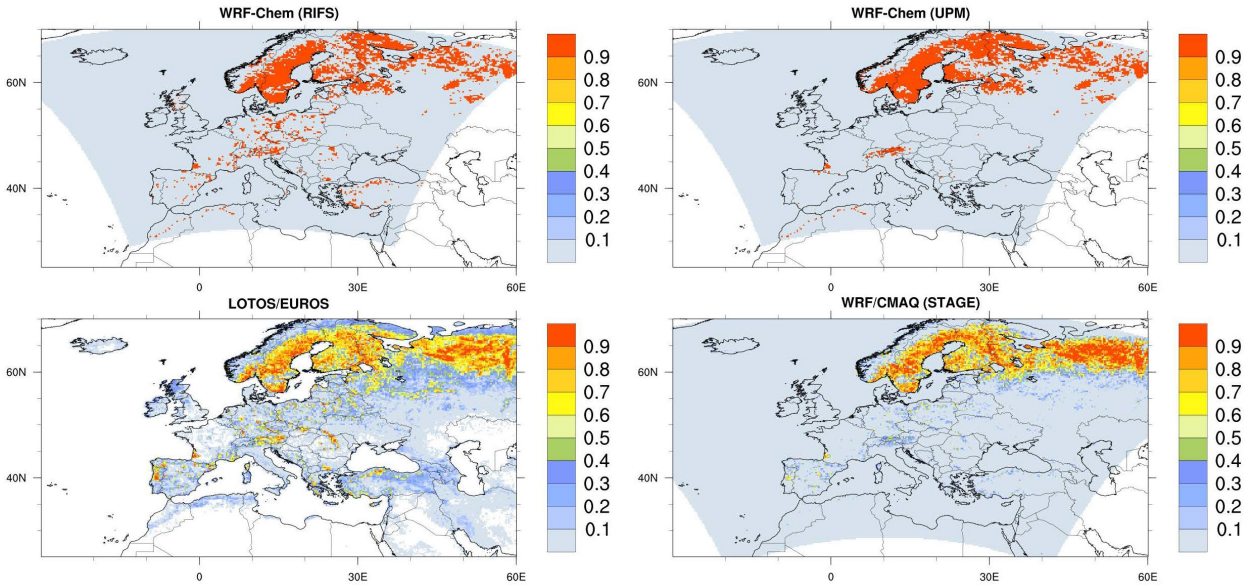

Figure S11: Fractional coverage of the evergreen needleleaf forest LU category for each of the participating models over the EU domain.

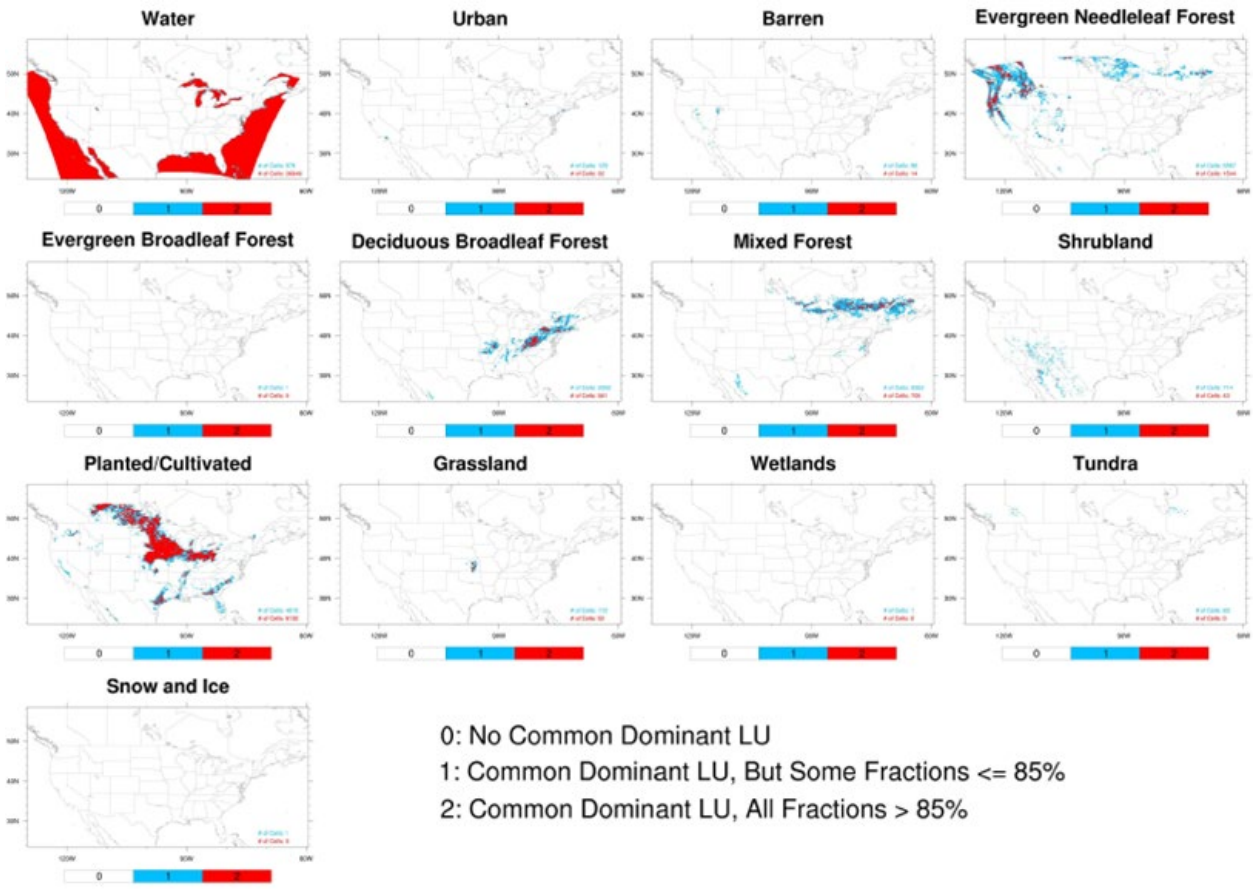

Figure S12: For each LU category, maps depicting the location of grid cells that i) do not share a common dominant LU category across models (white cells), ii) share a common dominant LU category across models but not all models have a fractional coverage > 85% for that LU category (blue cells), or iii) share a common dominant LU category across models and all models have a fractional coverage > 85% for that LU category (red). Results show are for the NA domain. The number of blue and red cells is shown as insert in each map. No maps are shown for the deciduous needleleaf forest, herbaceous, and savanna LU categories because there is not a single common dominant LU grid cell across models for these categories (see Table 5).

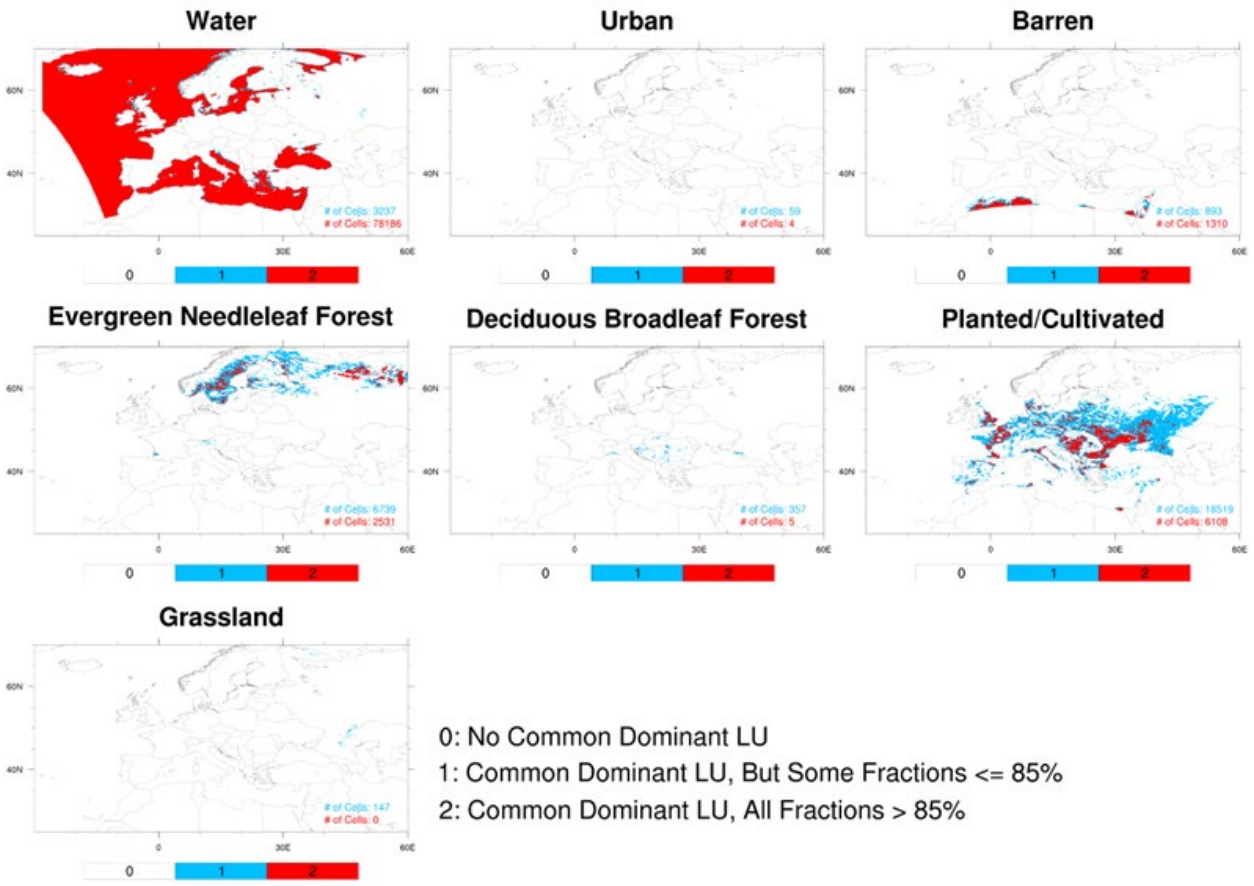

Figure S13. For each LU category, maps depicting the location of grid cells that i) do not share a common dominant LU category across models (white cells), ii) share a common dominant LU category across models but not all models have a fractional coverage > 85% for that LU category (blue cells), or iii) share a common dominant LU category across models and all models have a fractional coverage > 85% for that LU category (red). Results show are for the EU domain. The number of blue and red cells is shown as insert in each map. No maps are shown for the deciduous needleleaf forest, evergreen broadleaf forest, mixed forest, shrubland, herbaceous, savanna, wetlands, tundra, and snow and ice LU categories because there is not a single common dominant LU grid cell across models for these categories (see Table 5).

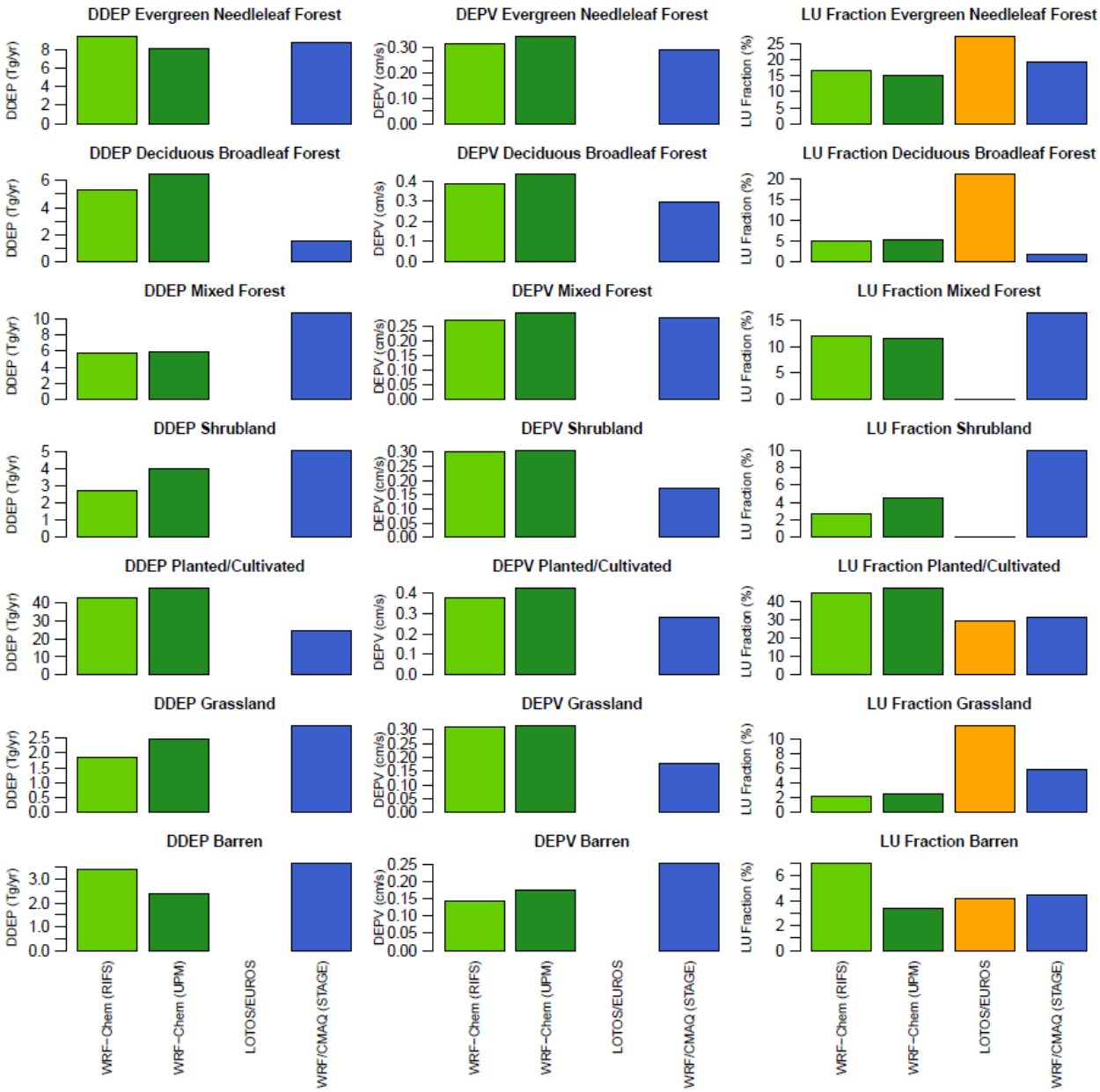

Figure S14. LU-specific annual domain-total dry deposition fluxes (Tg), LU-specific annual mean dry deposition velocity (cm/s), and percentage LU category domain coverage (excluding water grid cells) for seven selected LU categories over the EU domain. For each LU category and model, the analysis considered grid cells in the analysis domain common to all models in which a given model had at least 85% coverage for this LU category. The number of these grid cells differs across models due to underlying differences in LU (see Section 3.3).

References

Clifton, O. E., Schwede, D., Hogrefe, C., Bash, J. O., Bland, S., Cheung, P., Coyle, M., Emberson, L., Flemming, J., Fredj, E., Galmarini, S., Ganzeveld, L., Gazetas, O., Goded, I., Holmes, C. D., Horváth, L., Huijnen, V., Li, Q., Makar, P. A., Mammarella, I., Manca, G., Munger, J. W., Pérez-Camanyo, J. L., Pleim, J., Ran, L., San Jose, R., Silva, S. J., Staebler, R., Sun, S., Tai, A. P. K., Tas, E., Vesala, T., Weidinger, T., Wu, Z., and Zhang, L.: A single-point modeling approach for the intercomparison and evaluation of ozone dry deposition across chemical transport models (Activity 2 of AQMEII4), Atmos. Chem. Phys., 23, 9911–9961, https://doi.org/10.5194/acp-23-9911-2023, 2023